

Article

# Effects of Initial Grain Size of Al-Zn-Mg-Cu Alloy on the Recrystallization Behavior and Recrystallization Mechanism in Isothermal Compression

Jiuhui Zhao <sup>1</sup>, Yunlai Deng <sup>1,2</sup>, Fushun Xu <sup>3,4,\*</sup> and Jin Zhang <sup>1</sup>

<sup>1</sup> Light Alloy Research Institute, Central South University, Changsha 410083, China;

zjh\_aluminium@csu.edu.cn (J.Z.); luckdeng@csu.edu.cn (Y.D.); zhangjinlari@csu.edu.cn (J.Z.)

<sup>2</sup> State Key Laboratory of High Performance and Complex Manufacturing, Central South University, Changsha 410083, China

<sup>3</sup> Kunming Metallurgical Research Institute, Kunming 650031, China

<sup>4</sup> State Key Laboratory of Pressure Hydrometallurgical Technology of Associated Nonferrous Metal Resources, Kunming 650031, China

\* Correspondence: xuzhang1808@163.com; Tel.: +86-0731-88876913

Received: 27 December 2018; Accepted: 16 January 2019; Published: 22 January 2019



**Abstract:** Fine-grained (average grain size 3.8  $\mu\text{m}$ ) and coarse-grained (average grain size 24.9  $\mu\text{m}$ ) Al-Zn-Mg-Cu alloys were subjected to isothermal compression at  $10^{-3} \text{ s}^{-1}$  and temperature ranges from 300 °C to 450 °C. The grain structures after isothermal compression were observed by electron backscatter diffraction (EBSD). The results show that the continuous dynamic recrystallization (CDRX) mechanism dominated to form sub-grains in grain interiors during isothermal compression of coarse-grained materials, and sub-grains were gradually developed in grain interiors as the effective strain increased. Discontinuous dynamic recrystallization (DDRX) was the main recrystallization mechanism during isothermal compression of fine-grained materials, in which finer recrystallized grains were formed at grain boundaries. The temperature of isothermal compression had little influence on the recrystallization when the growth of recrystallized grains was slight, and sub-grains were hardly developed in fine-grain interiors.

**Keywords:** Al-Zn-Mg-Cu; isothermal compression; recrystallization; recrystallization mechanism

## 1. Introduction

Dynamic recrystallization has been studied extensively, including recrystallization in hot rolling [1,2], hot extrusion [3,4], and hot forging [5,6]. Generally, the finer grain structure of aluminum alloy brings better mechanical properties for enhancing grain boundary strengthening [7–10]. Roven et al. [11] found that the ultimate tensile strength increased significantly in a finer grain structure while the ductility almost remained the same. In addition, the grain structure of aluminum alloy containing mainly fine sub-grains, improving its corrosion resistance for precipitation free zones (PFZs), was hardly formed along low angle boundaries [12,13]. Naeini et al. [14] found that pitting corrosion resistance of 5052 aluminum alloys was diminished with a finer grain structure. Wei et al. [15] found that the size and the amount of pitting corrosion in an ultra-fine grained UFG Al-Mn alloy sample was lower compared to a coarse-grained (CG) sample. The grain structures are mainly controlled by dynamic recrystallization during hot deformation, thus it is important to understand dynamic recrystallization behavior and recrystallization mechanisms.

Isothermal compression of aluminum alloys has been studied for a long time to understand dynamic recrystallization behavior under various conditions [16–19]. Generally, recrystallized grains increase as the temperature of isothermal compression increases [20] or strain rate [21] decreases, but the average size of recrystallized grains increases slightly. Besides, isothermal

multi-direction forging (MDF) with continuous dynamic recrystallization (CDRX) mechanism has also been substantially reported in recent years, which is employed to grain refinement by transformation of lower angle grain boundaries (LAGBs) formed at early stages into higher angle grain boundaries (HAGBs) [22,23]. Another dynamic recrystallization mechanism is discontinuous dynamic recrystallization (DDRX), in which fine recrystallized grains were formed at grain boundaries [24].

The grain structure of material that is subjected to hot compression may have large differences with different situations; the grain structure may have big differences after isothermal compression. Although various initial materials with different grain sizes that are subjected to isothermal compression has been studied, the influence of grain size on recrystallization mechanisms and recrystallization behavior is not obvious. However, when the initial grain size of initial materials that are subjected to isothermal compression is small enough, the effect of the grain size of aluminum alloy on the recrystallization behavior and recrystallization mechanism during isothermal compression has not been reported until now. In order to fill this gap, Al-Zn-Mg-Cu alloys with an average grain size around 25  $\mu\text{m}$  or 4  $\mu\text{m}$  were subjected to isothermal compression to study the influence of grain size on the recrystallization behavior and recrystallization mechanism.

## 2. Material and Methods

The aluminum alloy used in this study was Al-5.47Zn-2.19Mg-2.11Cu-0.12Zr-0.01Cr-0.1Fe-0.01Mn (wt.%). Two different initial materials that were subjected to isothermal compression were produced by extrusion and equal-channel angular pressing (ECAP) of cylindrical samples (20 mm diameter by 100 mm long), respectively. The coarse-grained materials were processed by extrusion at 400  $^{\circ}\text{C}$  from a diameter 40 mm to 20 mm, and then they were subjected to solution heat treatment at 470  $^{\circ}\text{C}$  for 2 h and water quenched before isothermal compression. The fine-grained materials were produced by ECAP at 400  $^{\circ}\text{C}$  with twelve passes, and then they were subjected to solution heat treatment at 470  $^{\circ}\text{C}$  for 2 h and water quenched before isothermal compression. The EBSD maps of two different starting materials are shown in Figure 1. The average size of the coarse-grains materials was 68  $\mu\text{m}$  along the extrusion direction and 24.9  $\mu\text{m}$  perpendicular to the extrusion direction. The average size of the fine-grained materials was 3.8  $\mu\text{m}$  along the extrusion direction and 3.6  $\mu\text{m}$  perpendicular to the extrusion direction. For the sake of the initial materials with two different grain sizes, they were subjected to solid solution heat treatment at 470  $^{\circ}\text{C}$  for 2 h and adequate recrystallization occurred; the preliminary crystallographic was almost the same with cube texture.

Cylindrical specimens with a size of  $\Phi 7 \times 10 \text{ mm}^2$  was machined from the center of the extrusion materials and ECAP materials. Isothermal compression was carried out at strain rates of  $10^{-3} \text{ s}^{-1}$  and temperatures ranged from 300  $^{\circ}\text{C}$  to 450  $^{\circ}\text{C}$  to an effective strain of 1.2. These samples were heated to the target temperature at a rate of 20  $^{\circ}\text{C}/\text{s}$  and held for 5 min before compression. Isothermal compression was then performed on Gleeble-3500 with a lubricant powder of boron nitride, and rapid water quenching was performed after isothermal compression.

Microstructural analysis was carried out in the central part of the specimen, which was perpendicular to the compression axis, by electron backscattering diffraction pattern analysis using a field emission gun-environmental scanning electron microscopy (FEG-SEM, ZEISS, Berlin, Germany) FEI device equipped with an HKL Channel 5 EBSD system. The samples that isothermal compression for EBSD were prepared by electro polishing in a solution of 10%  $\text{HClO}_4$  and 90%  $\text{C}_2\text{H}_5\text{OH}$  at 20  $^{\circ}\text{C}$ , the step size during acquisition is 0.9. The EBSD data were collected using HKL Channel 5 software (version 1, ZEISS, Berlin, Germany). The average grain size were evaluated using the line-intercept technique, the low-angle boundaries (LABs) with  $2^{\circ}$  and  $15^{\circ}$  in the EBSD maps are depicted as thin lines while the high-angle boundaries (HABs)  $>15^{\circ}$  are depicted as thick lines.

The microstructure characterization was also carried out by transmission electron microscopy (TEM, FEI, Philadelphia, PA, USA) techniques in the central part of the specimen, which is perpendicular to the compression axis. The preparation of TEM is about 50  $\mu\text{m}$  foil, then the twin-jet

was polished in a 30% HNO<sub>3</sub> and 70% CH<sub>3</sub>OH solution. The TEM examination was performed using a Libra 200FE transmission electron microscope (FEI, Philadelphia, PA, USA) operating at 200 KV.

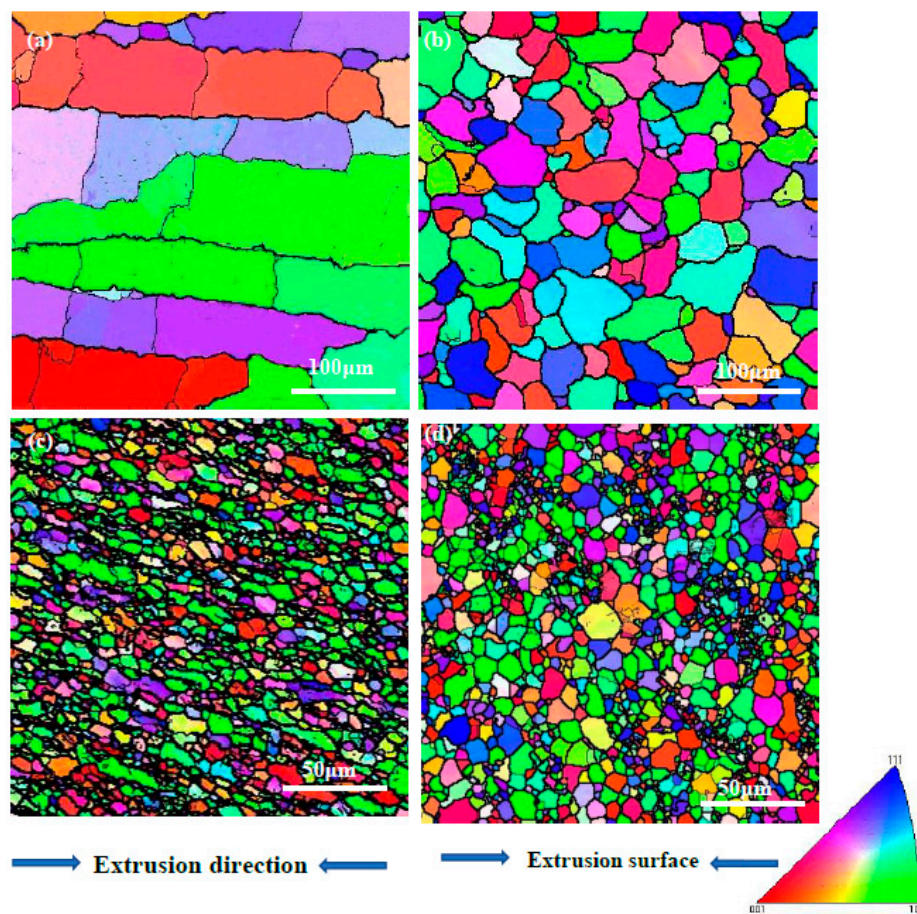
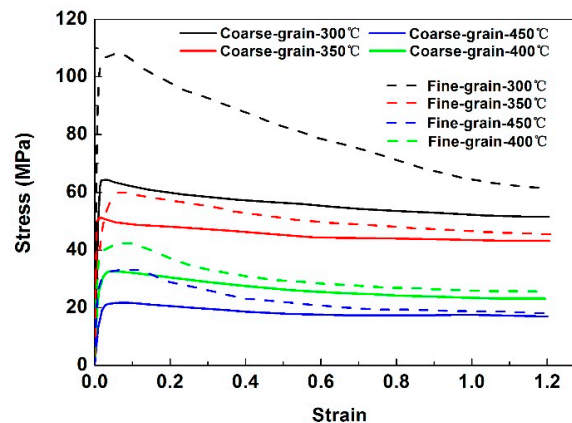


**Figure 1.** The initial EBSD maps that were subjected to isothermal compression: coarse-grained materials (a) along the extrusion direction, (b) perpendicular to the extrusion direction, and fine-grained materials (c) along the compression direction, (d) perpendicular to the compression direction.

### 3. Results

#### 3.1. Effect Initial Grain Size on the True Stress-Strain Curves during Isothermal Compression

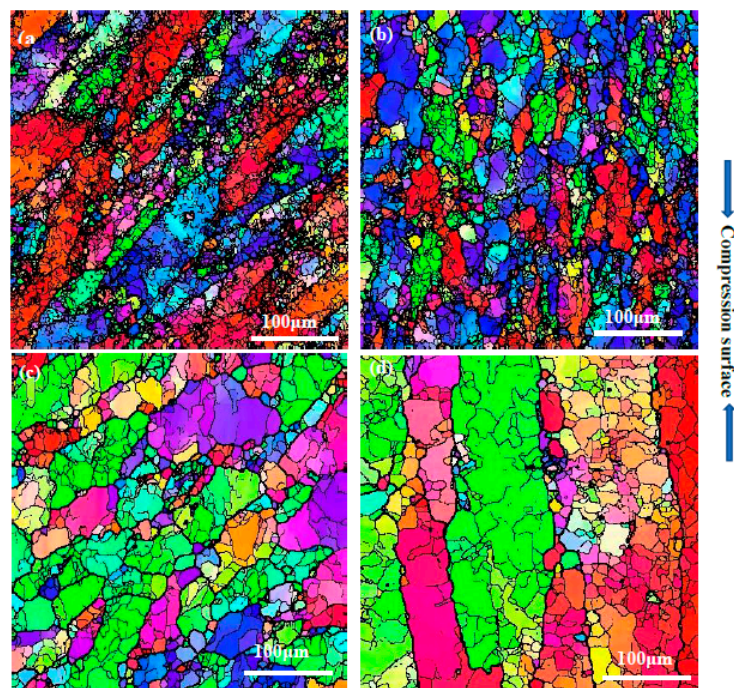
Fine-grained and coarse-grained aluminum alloy were subjected to isothermal compression at  $10^{-3} \text{ s}^{-1}$  and temperatures of 300 °C, 350 °C, 400 °C, and 450 °C to an effective strain of 1.2, the true stress-strain curves are shown in Figure 2. Two stages are included in these stress-strain curves, the effective stress increases to the maximum quickly at the first stage for increasing dislocations rapidly, and then drop gradually to be stable at the second stage for the occurrence of dynamic recrystallization or dynamic recovery to balance the number of dislocations. For coarse-grained alloy, the stress decreases gradually as the temperature increased from 300 °C to 450 °C during isothermal compression, and the maximum stress decreases from about 65 MPa to 20 MPa. Because the grain boundary strengthen is much stronger in fine-grained alloy than in the coarse-grained alloy, the true stress is much higher in the fine-grained alloy, and the maximum stress decreases gradually from 110 MPa to 30 MPa as the temperature increased from 300 °C to 450 °C.



**Figure 2.** True stress-strain curves when isothermal compression is at  $10^{-3} \text{ s}^{-1}$  and various temperatures with fine-grained materials and coarse-grained materials.

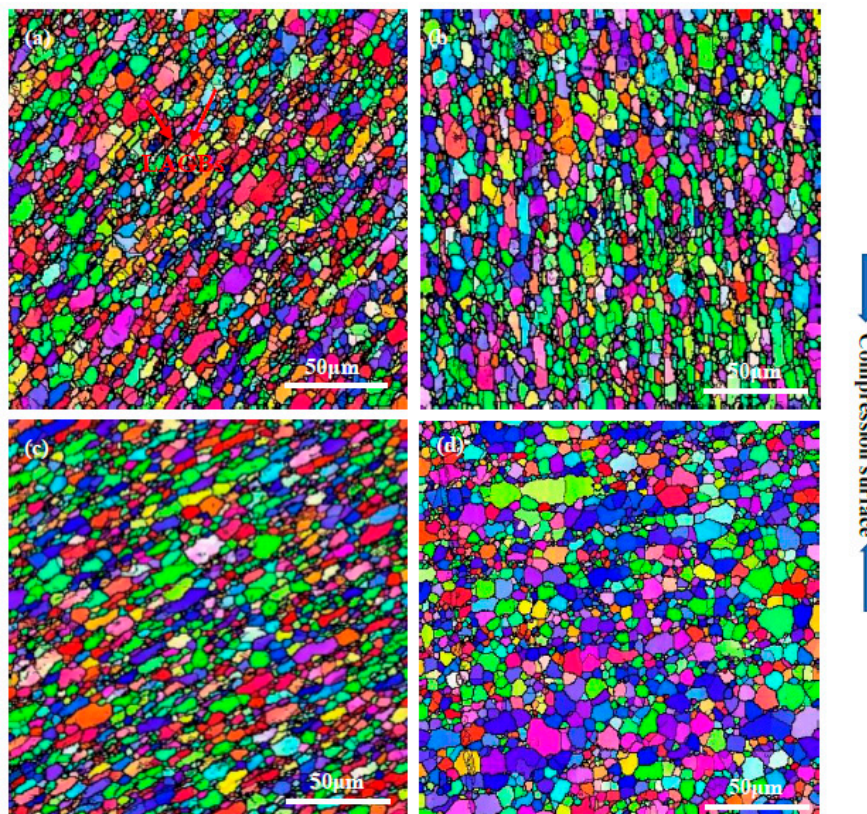
### 3.2. Effect of Initial Grain Size on Recrystallization after Isothermal Compression

Figure 3 shows the EBSD maps of our previous study [25] after isothermal compression of coarse-grained aluminum alloy at  $10^{-3} \text{ s}^{-1}$  and temperatures of 300 °C, 350 °C, 400 °C, and 450 °C. Many sub-grains were developed into grain interiors after isothermal compression. The number of sub-grains decreased, and the size of sub-grains increased gradually as the temperature of isothermal compression increased from 300 °C to 450 °C. A few recrystallized grains appeared in grain interiors, which are formed via increasing the misorientation of sub-grains. It is obvious that the CDRX mechanism is the main recrystallization mechanism for isothermal compression of coarse-grained materials, as many sub-grains are formed in grain interiors and a few of them are transferred into recrystallized grains, and almost none of the recrystallized grains are formed at grain boundaries [20,26].



**Figure 3.** EBSD maps after isothermal compression at  $10^{-3} \text{ s}^{-1}$  and various temperatures with coarse-grained materials: (a) 300 °C, (b) 350 °C, (c) 400 °C, (d) 450 °C. Compression surface means the surface is perpendicular to the compression axis.

As seen in Figure 4, totally different grain structures are formed after isothermal compression of the fine-grained aluminum alloy at  $10^{-3} \text{ s}^{-1}$  and temperatures of 300 °C, 350 °C, 400 °C, and 450 °C. After isothermal compression at 300 °C, almost a completely recrystallized grain structure is formed, only quite a few low angle grain boundaries (LAGBs) appear in grain interiors. As the temperature of isothermal compression increased from 300 °C to 450 °C, the grain structure did not change too much, and completely recrystallized grain structures were obtained. Discontinuous dynamic recrystallization is the main recrystallization mechanism, in which recrystallized grain are formed at grain boundaries, and almost no sub-grains are developed into fine grain interiors [21,26].



**Figure 4.** EBSD maps after isothermal compression at  $10^{-3} \text{ s}^{-1}$  and various temperatures with fine-grained materials: (a) 300 °C, (b) 350 °C, (c) 400 °C, and (d) 450 °C. Compression surface means the surface is perpendicular to the compression axis.

After isothermal compression of coarse-grained and fine-grained aluminum alloy at  $10^{-3} \text{ s}^{-1}$  and temperature ranges from 300 °C to 450 °C. Figure 5 shows the comparison of HAGB%, average grain size of sub-grains and recrystallized grains, and the percentage of misorientation angle of grain boundaries between  $3^\circ$  to  $27^\circ$ . For fine-grained materials, the HAGB% increases from 73.2% to 84.2% when the temperature of isothermal compression increased from 300 °C to 450 °C; it is much higher than with isothermal compression of coarse-grained materials. For coarse-grained materials, the HAGB% increases from 18.7% to 36.2% when the compression temperature increased from 300 °C to 450 °C. For coarse-grained alloy, a great many sub-grains were developed in the grain interiors, the average size of sub-grains increases from 3.3  $\mu\text{m}$  to 9.1  $\mu\text{m}$  as the temperature of isothermal compression increased from 300 °C to 450 °C. For fine-grained alloy, the average size of recrystallized grains increases from 3.7  $\mu\text{m}$  to 4.2  $\mu\text{m}$  slightly as the temperature increased from 300 °C to 450 °C, and it is smaller than the average size of sub-grains with isothermal compression of coarse-grained materials. The percentage of the misorientation angle of grain boundaries between  $3^\circ$  to  $27^\circ$  has great difference with isothermal compression of different initial materials; it is about 50% with isothermal

coarse-grained materials at temperature ranges from 300 °C to 450 °C, and it is about 27% with isothermal compression of fine-grained materials at temperature ranges from 300 °C to 450 °C.

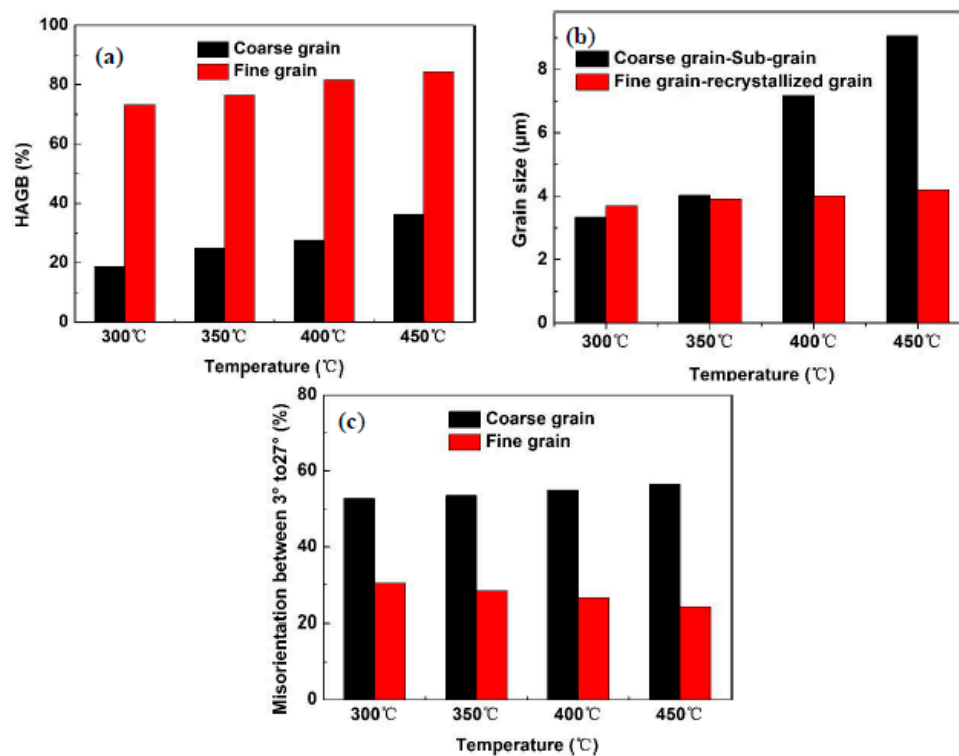


**Figure 5.** Comparison of (a) HAGB%, (b) grain size, and (c) misorientation angle of grain boundaries between 3° to 27° after isothermal compression fine-grained and coarse-grained materials at  $10^{-3} \text{ s}^{-1}$  and different temperatures.

## 4. Discussion

### 4.1. Effect of the Initial Grain Structure on the Dynamic Recrystallization Mechanism

Isothermal compression was performed at  $10^{-3} \text{ s}^{-1}$  and temperature ranges from 300 °C to 450 °C for coarse-grained materials. The CDRX mechanism dominated to form sub-grains in the grain interiors, as seen in Figure 3. The size of the sub-grains can be written as Equation (1).

$$D = k_1 - k_2 \log Z \quad (1)$$

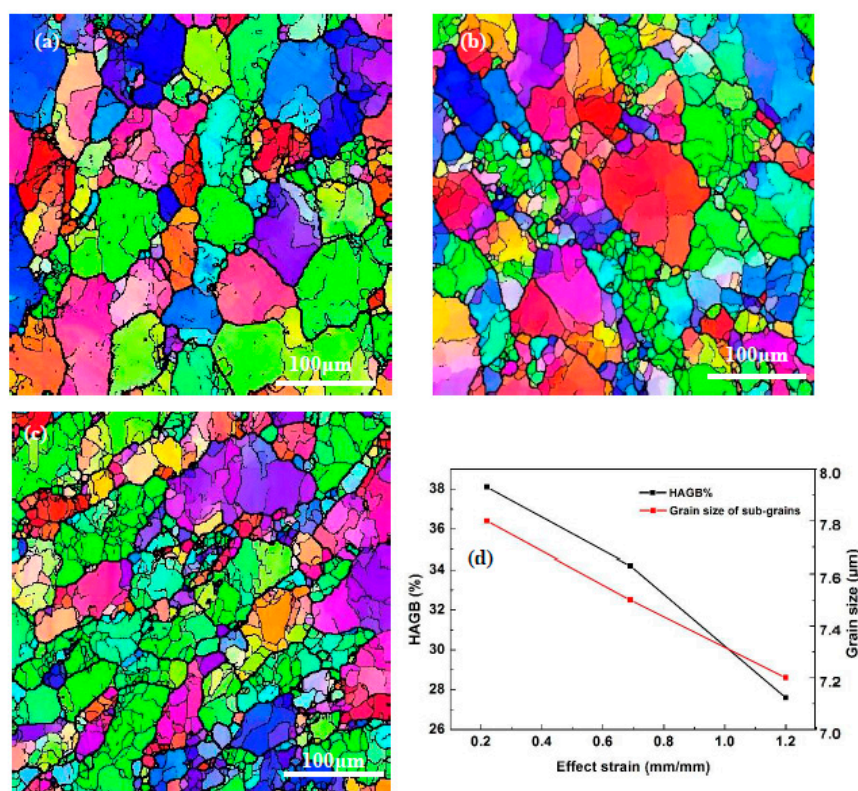
where  $k_1$  and  $k_2$  are constants,  $D$  is the sub-grains' size, and  $Z$  is the Zener–Hollomon parameter [27].

For the sake of the  $Z$  value decreasing as the temperature increases, the  $D$  value would increase when the temperature increases. Thus, the average size of the sub-grains increased gradually when the temperature of isothermal compression increased from 300 °C to 450 °C, as seen in Figure 5b.

However, when the temperature of isothermal compression was performed at  $10^{-3} \text{ s}^{-1}$  for fine-grained materials, almost no sub-grains were developed in grain interiors, as seen in Figure 4. The DDRX mechanism dominated to form recrystallized grains at grain boundaries. If sub-grains can develop in grain interiors with isothermal compression of fine-grained materials, as seen in Equation (1), the size of the sub-grains that formed with isothermal compression of fine-grained materials should be close to the size of sub-grains formed with isothermal compression of coarse-grained materials which shared the same  $Z$  value. But the average grain size with isothermal compression of fine-grained materials is smaller than the average sub-grain size with isothermal compression of coarse-grained materials, as seen in Figure 5b, thus almost no sub-grains were developed in grain interiors.

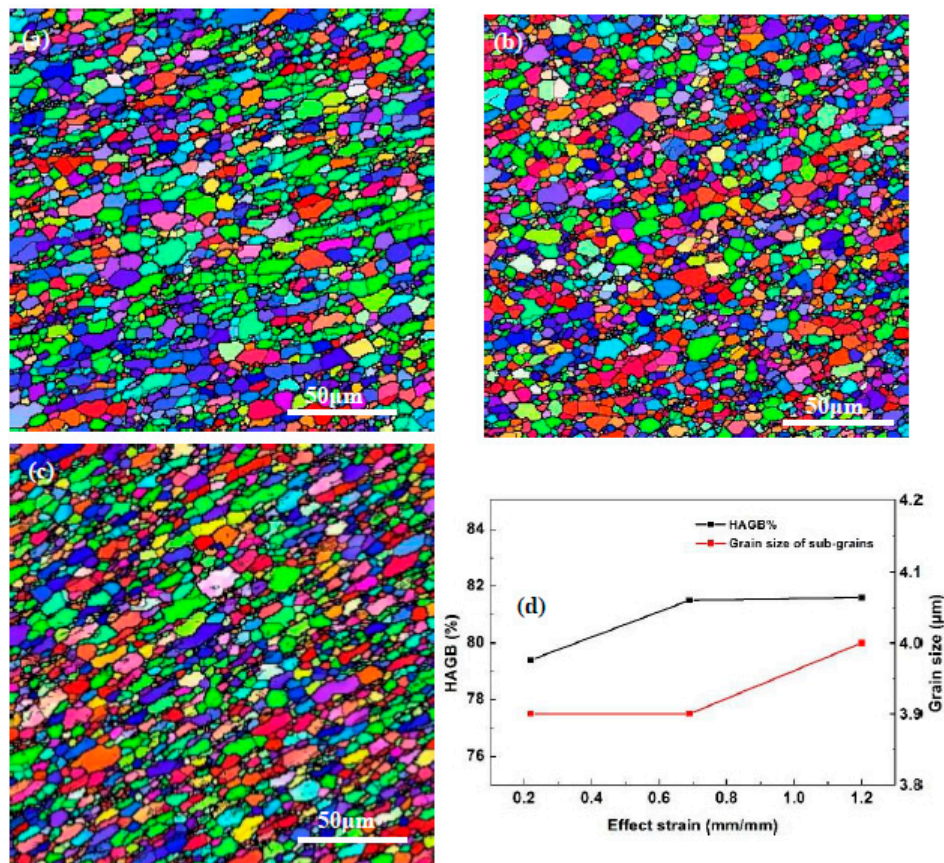
#### 4.2. The Evolution of Grain Structure with Two Different Dynamic Recrystallization Mechanisms

Figure 6 shows the evolution of grain structure with isothermal compression of coarse-grained materials at  $10^{-3} \text{ s}^{-1}$  and  $400 \text{ }^\circ\text{C}$ . For the effective strain of 0.22, Figure 6a shows that only a few sub-grains are formed near grain boundaries. As the effective strain increased from 0.22 to 1.2, the HAGB% decreases from 38.1% to 27.6%, and many more sub-grains were developed in the grain interiors with higher effective strain. Besides, the average sub-grain size decreased slowly from  $7.8 \text{ }\mu\text{m}$  to  $7.2 \text{ }\mu\text{m}$ . In addition, the coarse grains consisted of a higher density of dislocations which were sorted into walls and were transferred into sub-grains as effective strain increased. Also, the initial state of coarse grains includes low fraction of HAGBs and promoted the mobility of grain boundaries. Figure 5c shows the higher mobility with isothermal compression of coarse-grained materials. Therefore, sub-grains are continuously formed in grain interiors as effective strain increased during isothermal compression when CDRX is the main mechanism.



**Figure 6.** The EBSD maps with isothermal compression of coarse-grained materials at  $10^{-3} \text{ s}^{-1}$  and  $400 \text{ }^\circ\text{C}$  with different effective strains: (a) 0.22, (b) 0.69, (c) 1.2, and (d) related grain characterizations.

Figure 7 shows the evolution of grain structure with isothermal compression of fine-grained materials at  $10^{-3} \text{ s}^{-1}$  and  $400 \text{ }^\circ\text{C}$ . Almost completely recrystallized grain structures were obtained with isothermal compression of fine-grained materials at  $10^{-3} \text{ s}^{-1}$  with different effective strains. The HAGB% and the average grain size do not change too much as the effective strain increased from 0.22 to 1.2, the HAGB% is around 80% and the average grain size is about  $4 \text{ }\mu\text{m}$ . Figure 8 shows that the grain size after isothermal compression with different effective strains was between  $1 \text{ }\mu\text{m}$  to  $30 \text{ }\mu\text{m}$ , and 70% of grains after compression were between  $3 \text{ }\mu\text{m}$  to  $10 \text{ }\mu\text{m}$ . As effective strain increased from 0.22 to 1.2, finer grains with grain size approximately  $2.5 \text{ }\mu\text{m}$  increased gradually, for recrystallized grains formed at grain boundaries increased gradually. As the microstructure included fine grains, dislocation mobility was hindered and grain boundaries acted as barriers and sometimes sinks, thus sub-grains hardly formed. Figure 5c also shows the lower mobility of grain boundaries with isothermal compression of fine-grained materials.



**Figure 7.** The EBSD maps of isothermal compression of fine-grained materials at  $10^{-3} \text{ s}^{-1}$  and  $400 \text{ }^\circ\text{C}$  with different effective strains: (a) 0.22, (b) 0.69, (c) 1.2, and (d) related grain characterizations.

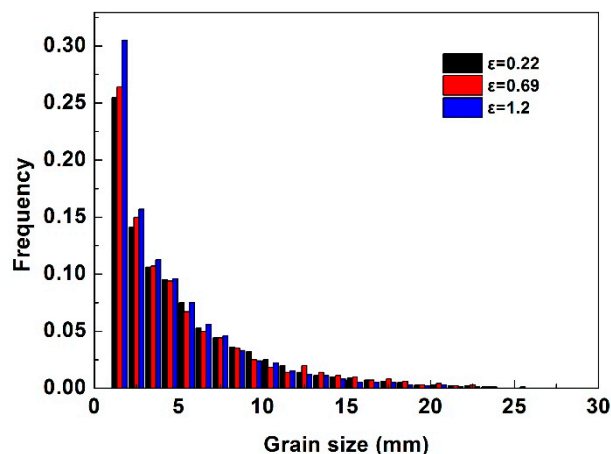


**Figure 8.** The grain distribution when isothermal compression of fine-grained materials with different effective strain.

#### 4.3. The TEM Maps when Isothermal Compression with Two Different Dynamic Recrystallization Mechanisms

Figure 9a shows that dislocation walls and low angle grain boundaries (LAGBs) are formed after isothermal compression of coarse-grained materials at  $400 \text{ }^\circ\text{C}$ . Many sub-grains were also formed which transferred from dislocation walls when the CDRX mechanism dominated, as seen in Figure 9b. When isothermal compression was performed on the fine-grained materials, dislocations were easier to move to grain boundaries during isothermal compression due to shorter grain boundary distance, leading to grain boundary bulging occurring to form DDRX grains. Thus, almost no sub-grains were formed with isothermal compression of fine-grained alloys. Figure 9b shows finer recrystallized

grains were formed at grain boundaries via the DDRX mechanism with isothermal compression of fine-grained materials at 400 °C.

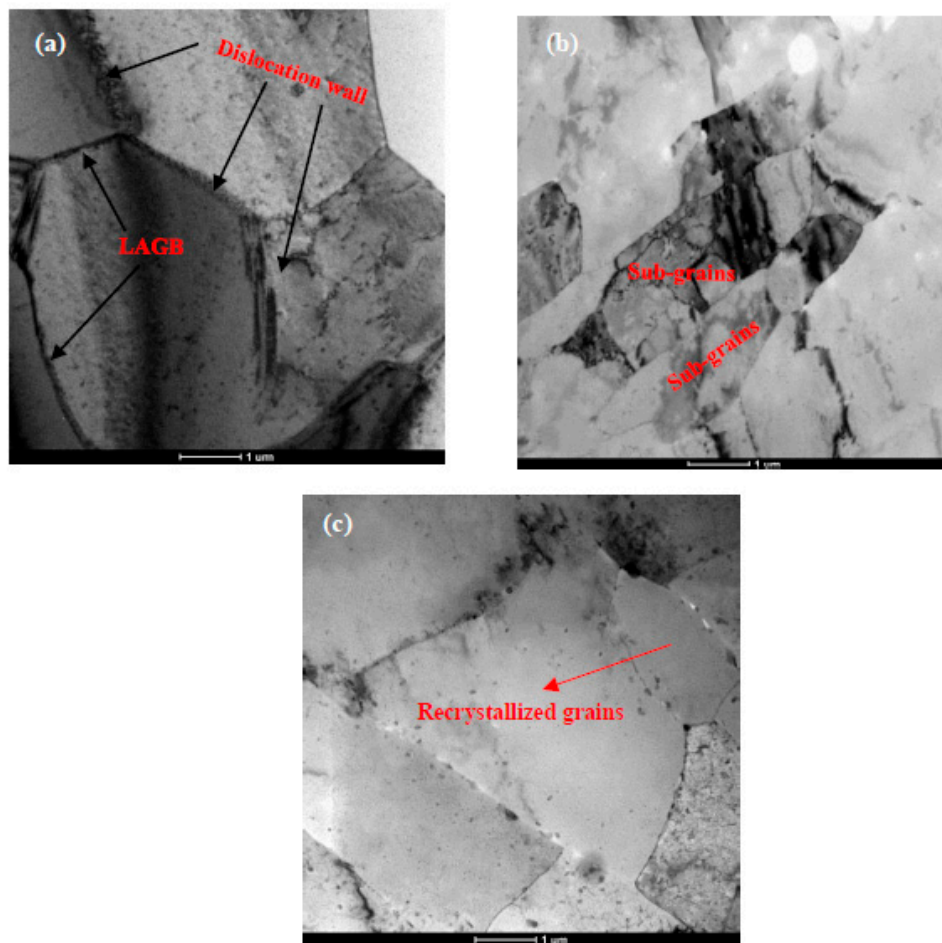


**Figure 9.** TEM maps after isothermal compression at 400 °C with different starting materials: (a) LAGB (low angle grain boundary) and dislocation wall in coarse-grained materials, (b) coarse-grained materials, and (c) fine-grained materials.

## 5. Conclusions

The effect of grain size on the recrystallization behavior and recrystallization mechanism during isothermal compression at  $10^{-3} \text{ s}^{-1}$  and temperature ranges from 300 °C to 400 °C were studied in Al-Zn-Mg-Cu alloy. The main conclusions are as follows:

- (1) When isothermal compression was performed on coarse-grained materials, the CDRX mechanism dominated to form sub-grains in grain interiors. The HAGB% and the average size of sub-grains increased gradually as the temperature of isothermal compression increased. However, DDRX was the main recrystallization mechanism when the starting material was fine-grained alloy, and many finer recrystallized grains were formed at grain boundaries with few sub-grains developed into grain interiors. The HAGB% and average size of recrystallized grains almost kept the same as the temperature increased.
- (2) The average grain size after isothermal compression of fine-grained materials was smaller than the average size of sub-grains after isothermal compression of coarse-grained materials. In addition, coarse sub-grains cannot be formed in fine grain interiors, thus almost no sub-grains were developed in fine grain interiors with isothermal compression of fine-grained materials.

**Author Contributions:** Investigation, J.Z. (Jiuhui Zhao) and Y.D.; Methodology, F.X.; Project administration, J.Z. (Jin Zhang); Writing—original draft, J.Z. (Jiuhui Zhao); Writing—review & editing, F.X.

**Funding:** This work was supported by the National Basic Research Program of China (No. 2017YFB0306301) and the National Natural Science Foundation of China (No. 51705539).

**Conflicts of Interest:** The authors declare no conflict of interest.

## References

1. Kumar, R.V.; Keshavamurthy, R.; Perugu, C.S.; Koppad, P.G.; Alipour, M. Influence of hot rolling on microstructure and mechanical behaviour of Al6061-ZrB2 in-situ metal matrix composites. *Mater. Sci. Eng. A* **2015**, *738*, 344–352.
2. Nayan, N.; Mishra, S.; Prakash, A.; Murty, S.V.S.N.; Prasad, M.J.N.V.; Samajdar, I. Effect of cross-rolling on microstructure and texture evolution and tensile behavior of aluminium-copper-lithium (AA2195) alloy. *Mater. Sci. Eng. A* **2019**, *740*, 252–261.
3. Wang, X.; Pan, Q.; Liu, L.; Xiong, S.; Wang, W.; Lai, J.; Huang, Z. Characterization of hot extrusion and heat treatment on mechanical properties in a spray formed ultra-high strength Al-Zn-Mg-Cu alloy. *Mater. Charact.* **2018**, *144*, 131–140.
4. Che, H.; Jiang, X.; Qiao, N.; Liu, X. Effects of Er/Sr/Cu additions on the microstructure and mechanical properties of Al-Mg alloy during hot extrusion. *J. Alloys Compd.* **2017**, *708*, 662–670.
5. Zhang, Y.; Jiang, S.; Zhao, Y.; Shan, D. Isothermal precision forging of complex-shape rotating disk of aluminum alloy based on processing map and digitized technology. *Mater. Sci. Eng. A* **2013**, *580*, 294–304.
6. Zhang, Y.; Jiang, S.; Zhao, Y.; Shan, D. Isothermal precision forging of aluminum alloy ring seats with different preforms using FEM and experimental investigation. *Int. J. Adv. Manuf. Technol.* **2014**, *72*, 1693–1703.
7. Ma, K.; Wen, H.; Hu, T.; Topping, T.D.; Isheim, D.; Seidman, D.N.; Schoenung, J.M. Mechanical behavior and strengthening mechanisms in ultrafine grain precipitation-strengthened aluminum alloy. *Acta Mater.* **2014**, *62*, 141–155.
8. Lee, S.H.; Saito, Y.; Sakai, T.; Utsunomiya, H. Microstructures and mechanical properties of 6061 aluminum alloy processed by accumulative roll-bonding. *Mater. Sci. Eng. A* **2002**, *325*, 228–235.
9. Zhao, Y.H.; Liao, X.Z.; Jin, Z.; Valiev, R.Z.; Zhu, Y.T. Microstructures and mechanical properties of ultrafine grained 7075 Al alloy processed by ECAP and their evolutions during annealing. *Acta Mater.* **2004**, *52*, 4589–4599.
10. Eizadjou, M.; Manesh, H.D.; Janghorban, K. Microstructure and mechanical properties of ultra-fine grains (UFGs) aluminum strips produced by ARB process. *J. Alloys Compd.* **2009**, *474*, 406–415.
11. Roven, H.J.; Nesboe, H.; Werenskiold, J.C.; Seibert, T. Mechanical properties of aluminium alloys processed by spd: comparison of different alloy systems and possible product areas. *Mater. Sci. Eng. A* **2005**, *410*, 426–429. [[CrossRef](#)]
12. Deng, Y.; Yin, Z.; Zhao, K.; Duan, J.; Hu, J.; He, Z. Effects of Sc and Zr microalloying additions and aging time at 120 C on the corrosion behaviour of an Al-Zn-Mg alloy. *Corros. Sci.* **2012**, *65*, 288–298. [[CrossRef](#)]
13. Tanaka, H.; Minoda, T. Mechanical properties of 7475 aluminum alloy sheets with fine subgrain structure by warm rolling. *Trans. Nonferrous Metals Soc. China* **2014**, *24*, 2187–2195. [[CrossRef](#)]
14. Naeini, M.F.; Shariat, M.H.; Eizadjou, M. On the chloride-induced pitting of ultra fine grains 5052 aluminum alloy produced by accumulative roll bonding process. *J. Alloys Compd.* **2011**, *509*, 4696–4700. [[CrossRef](#)]
15. Wei, W.; Wei, K.X.; Du, Q.B. Corrosion and tensile behaviors of ultra-fine grained Al-Mn alloy produced by accumulative roll bonding. *Mater. Sci. Eng. A* **2007**, *454*, 536–541. [[CrossRef](#)]
16. Luo, J.; Li, M.Q.; Ma, D.W. The deformation behavior and processing maps in the isothermal compression of 7A09 aluminum alloy. *Mater. Sci. Eng. A* **2012**, *532*, 548–557. [[CrossRef](#)]
17. Wu, B.; Li, M.Q.; Ma, D.W. The flow behavior and constitutive equations in isothermal compression of 7050 aluminum alloy. *Mater. Sci. Eng. A* **2012**, *542*, 79–87. [[CrossRef](#)]
18. Wu, H.; Wen, S.P.; Huang, H.; Wu, X.L.; Gao, K.Y.; Wang, W.; Nie, Z.R. Hot deformation behavior and constitutive equation of a new type Al-Zn-Mg-Er-Zr alloy during isothermal compression. *Mater. Sci. Eng. A* **2016**, *651*, 415–424. [[CrossRef](#)]
19. Lin, Y.C.; Li, L.T.; Xia, Y.C.; Jiang, Y.Q. Hot deformation and processing map of a typical Al-Zn-Mg-Cu alloy. *J. Alloys Compd.* **2013**, *550*, 438–445. [[CrossRef](#)]
20. Liu, W.; Zhao, H.; Li, D.; Zhang, Z.; Huang, G.; Liu, Q. Hot deformation behavior of AA7085 aluminum alloy during isothermal compression at elevated temperature. *Mater. Sci. Eng. A* **2014**, *596*, 176–182. [[CrossRef](#)]

21. Yang, Q.; Deng, Z.; Zhang, Z.; Liu, Q.; Jia, Z.; Huang, G. Effects of strain rate on flow stress behavior and dynamic recrystallization mechanism of Al-Zn-Mg-Cu aluminum alloy during hot deformation. *Mater. Sci. Eng. A* **2016**, *662*, 204–213. [[CrossRef](#)]
22. Sitdikov, O.; Garipova, R.; Avtokratova, E.; Mukhametdinova, O.; Markushev, M. Effect of temperature of isothermal multidirectional forging on microstructure development in the Al-Mg alloy with nano-size aluminides of Sc and Zr. *J. Alloys Compd.* **2018**, *746*, 520–531. [[CrossRef](#)]
23. Sakai, T.; Miura, H.; Goloborodko, A.; Sitdikov, O. Continuous dynamic recrystallization during the transient severe deformation of aluminum alloy 7475. *Acta Mater.* **2009**, *57*, 153–162. [[CrossRef](#)]
24. Cram, D.G.; Zurob, H.S.; Brechet, Y.J.M.; Hutchinson, C.R. Modelling discontinuous dynamic recrystallization using a physically based model for nucleation. *Acta Mater.* **2009**, *57*, 5218–5228. [[CrossRef](#)]
25. Zhao, J.; Deng, Y.; Tan, J.; Zhang, J. Effect of strain rate on the recrystallization mechanism during isothermal compression in 7050 aluminum alloy. *Mater. Sci. Eng. A* **2018**, *734*, 120–128. [[CrossRef](#)]
26. Huang, K.; Logé, R.E. A review of dynamic recrystallization phenomena in metallic materials. *Mater. Des.* **2016**, *111*, 548–574. [[CrossRef](#)]
27. Humphreys, F.J.; Hatherly, M. Chapter 13—hot deformation and dynamic restoration. In *Recrystallization & Related Annealing Phenomena*; Elsevier: Amsterdam, The Netherlands, 2004; pp. 415–450.



© 2019 by the authors. Licensee MDPI, Basel, Switzerland. This article is an open access article distributed under the terms and conditions of the Creative Commons Attribution (CC BY) license (<http://creativecommons.org/licenses/by/4.0/>).